Evolution of cell resistance, threshold voltage and crystallization temperature during cycling of line-cell phase-change random access memory

J. L. M. Oosthoek,[1,a)] K. Attenborough,[2] G. A. M. Hurkx,[2] F. J. Jedema,[2] D. J. Gravesteijn,[2] and B. J. Kooi[1]
[1]*Materials innovation institute M2i and Zernike Institute for Advanced Materials, University of Groningen, Nijenborgh 4, 9747 AG, Groningen, The Netherlands*
[2]*NXP-TSMC Research Center, Kapeldreef 75, 3001 Leuven, Belgium*

(Received 28 February 2011; accepted 23 May 2011; published online 22 July 2011)

Doped SbTe phase change (PRAM) line cells produced by *e*-beam lithography were cycled 100 million times. During cell cycling the evolution of many cell properties were monitored, in particular the crystalline and amorphous resistance, amorphous resistance drift exponent, time-dependent threshold voltage, threshold voltage as a function of RESET pulse height, crystallization temperature, and activation energy of crystal growth. The power of the present approach is that all these properties were measured simultaneously during the life of single cells. The evolution of the cell properties can be summarized by (i) an initialization phase characterized by settle-in effect of the material surrounding the programmable region, (ii) a usable life phase where initially the cell properties remain fairly constant until after $\sim 5 \times 10^5$ cycles decomposition of the programmed region caused degradation of the cell properties, and (iii) finally an end of life phase where the cell is stuck in the SET state after typically 10^8 cycles. Although generally the threshold voltage is directly related to the amorphous resistance it was found that during cycling this relation is not constant but evolved as well. Instead, the crystallization temperature could be linked to the threshold voltage throughout the complete life cycle of the cell which could lead to new insights to the nature of the threshold event. [doi:10.1063/1.3603025]

I. INTRODUCTION

Phase change random access memory (PRAM) is considered to be one of the most promising candidates for future non-volatile memories.[1] Its application ranges from mass data storage to embedded memories in, for instance, *smart cards* and automotive integrated circuits. For the embedded memories the so-called line-cell geometry was proposed by NXP.[2] Line-cells typically have a larger foot print compared to vertical cells (Ovonic universal memory, OUM)[3] and are thus less suitable for mass data storage. However for embedded memory applications this is compensated by the minimum impact on a standard CMOS process: Only three additional lithographic steps are necessary. Furthermore, due to the planar geometry the programming current scales with the phase change layer thickness and linewidth, rather than with the minimum lithography feature size only. Although sub-lithographic features are possible[4] and will most likely be mandatory for mass data storage applications, the easy processability and reduction of energy consumption with layer thickness make line-cells an ideal candidate for low-cost applications where less memory density is not critical.

PRAM exploits the large (three to four orders of magnitude) difference in electrical resistance of the amorphous and crystalline states of phase-change materials, which are renowned for their extremely fast crystallization kinetics at high temperatures and stability at operating temperatures.[1] A fast, high-energy pulse transforms the crystalline cell into an amorphous state by melt-quenching. The crystalline state can be recovered by applying a longer low-energy pulse that heats the cell, optimally below the melting temperature. The higher mobility of the atoms allows crystallization of the amorphous region during the pulse. This can also be performed fast, within 100 ns, but not as fast as melt-quenching that can in principle be performed with subpicoseconds pulses.[5,6]

The amorphous phase displays peculiar properties such as threshold switching[7] and temporal drift of the resistance and threshold voltage of the amorphous phase[8–10] that are critical for the PRAM behavior. The threshold event by itself does not crystallize the cell and has been explained in literature by either an electrical switching phenomenon[8,9] related to trap kinetics and electron recombination or to the creation of crystalline filaments.[10,11] In the absence of crystal growth and nucleation, which is predominant at elevated temperatures, the amorphous resistance continuously increases (drift) as a function of time even at room temperature. This is ideal for a memory based on two distinct stable states since (in the absence of crystallization) the read window improves in time. However for multilevel memory applications based on programming the cell to different amorphous states[12,13] within the continuum of three to four orders of magnitude this creates the possibility that one state drifts into the resistance window of the next state. The temporal drift of the threshold voltage, which also corresponds to a continuous increase with time,[8–10] can complicate the operation of

a)Author to whom correspondence should be addressed. Electronic mail: jasper.l.m.oosthoek@gmail.com.

PRAM. Therefore it is imperative that the maximum expected value does not exceed the operation voltage of the memory.

Accurate knowledge and understanding of these phenomena and the critical properties of non-volatile memories, including data retention (archive stability), program settings (voltages and currents needed to switch between the two or multilevel states of the memory) and cyclability (endurance), are essential for the PRAM technology. Published line cell endurance is currently limited to one hundred million cycles.[14] Within this limit all the other properties of the memory should ideally be independent of the cycle number. In this work we show detailed results on the evolution of memory cell characteristics during cycling. We measured the resistances, resistance drift, threshold voltage, threshold-voltage drift, crystallization temperature, and activation energy for crystallization during cycling. The uniqueness and novelty of the present work is that all these properties have been obtained simultaneously for a single cell with excellent reproducibility when repeating for several cells. Generally the evolution of a single property, like the threshold voltage, with cell cycling is measured.[8] This enables us, to determine more accurately the interdependencies of several parameters.

Here, we demonstrate the usefulness of this approach by showing that during cycling the threshold voltage and crystallization temperature of the phase-change material both decrease and follow a remarkable similar evolution. Generally, it is assumed and also demonstrated[8] that the threshold voltage and the amorphous phase resistance are linked in a rigid way. We show that in our measurements the amorphous resistance is not the dominating factor for predicting the threshold voltage. We relate the decrease in threshold voltage and crystallization temperature as cycling progresses to decomposition of the phase-change material. Finally the cell becomes stuck in the (crystalline) SET state after typically 10 to 100 million cycles.

II. EXPERIMENTAL

Phase change line cells of dimension $15 \times 75 \times 225$ nm^3 were produced by e-beam lithography (see TEM image in Fig. 1). The devices were fabricated on (100) Si wafers with a 500 nm grown thermal oxide layer. First, TiW bottom electrodes are deposited and patterned by standard optical lithography. Subsequently an oxide layer is deposited and the surface is planarized by a chemical mechanical polishing (CMP) step. After CMP, the TiW electrodes were cleaned by an *in situ* sputter etch after which a 15 nm doped SbTe phase change layer was sputter deposited at room temperature. Single line cells are then patterned by *e*-beam lithography and Ar plasma etching, using a hydrogen silsesquioxane (HSQ) hard mask and then passivated by oxide. More processing details can be found elsewhere.[15]

Wafer pieces containing cells are mounted on a ceramic plate with built-in heating filament and thermocouple allowing for a fast and accurate control of the cell temperature. The temperature is controlled with a PID controller and a controllable DC power supply connected to the heating filament. The temperature is kept stable to $\pm 0.1\,^{\circ}$C.

The total measurement setup is schematically depicted in Fig. 2(d). Contact to the cell was made by a custom built dual probe needle system with a 3.2 kΩ series resistor connected close to the needle. This series resistor limits the SET current after the threshold event and simulates the selection transistor in a memory. A Tektronix AFG3102 arbitrary function generator was used as a pulse generator which can produce any combination (and shape) of SET, RESET and read pulses with pulse edges down to 4 ns. Pulse voltage and currents were monitored by an Agilent DSO6052 A digital storage oscilloscope which also provides 50 Ω termination. The cell resistance was measured accurately with a Keithley 2601 source meter. An RF switch selects between the current channel of the oscilloscope and the source meter [Fig. 2(d)].

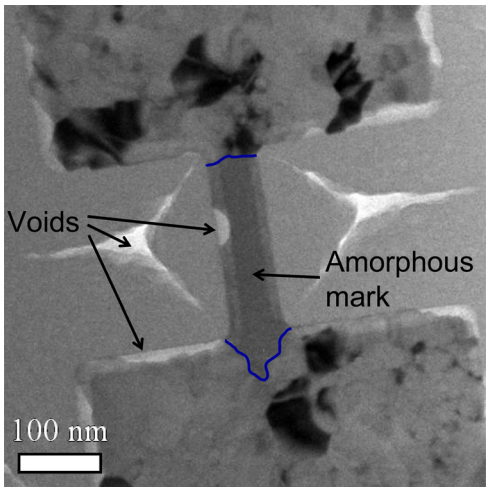

FIG. 1. (Color online) Plan-view TEM image of an FIB processed line cell with dimensions $15 \times 50 \times 250$ nm^3 showing the RESET state with a large amorphous mark. Except for the slightly different dimensions this cell is identical to the cells characterized in this study.

A complete switching cycle consists *either* of a single RESET [see Fig. 2(a)] and SET pulse [see Fig. 2(b)], where the cell resistance is measured with the source meter after both the RESET and the SET pulse, *or* a single RESET-read-SET-read pulse sequence [see Fig. 2(c)], where a complete cycle is performed with a single programmed pulse from the arbitrary function generator which can be repeated up to a million times.

A. Accurate RESET/SET cycle

After a single RESET pulse [Fig. 2(a)] the resistance is measured for 10 s as a function of time with exponentially increasing intervals after the RESET event (inset of Fig. 3(a)). It is a well known fact that the amorphous resistance exhibits a time dependence.[8] It increases (drifts) in time and follows a well established power law $R_t = R_1 \cdot (t/t_0)^{\alpha}$ where R_1 is the resistance at $t_0 = 1$ s after RESET and α is an empirical power law coefficient.[8] From the resistance measurements both R_1 and α were obtained. After the 10 s drift the arbitrary function generator is reprogrammed and a single SET pulse [Fig. 2(b)] crystallizes the cell. The SET pulse has long (200 ns) leading and trailing edges. The long leading edge allows for a measurement of threshold voltage. The current increases suddenly during the threshold event (faster than the measurement limit of our equipment). The 200 ns trailing edge avoids large capacitive currents related to the ~pF stray capacitance of the

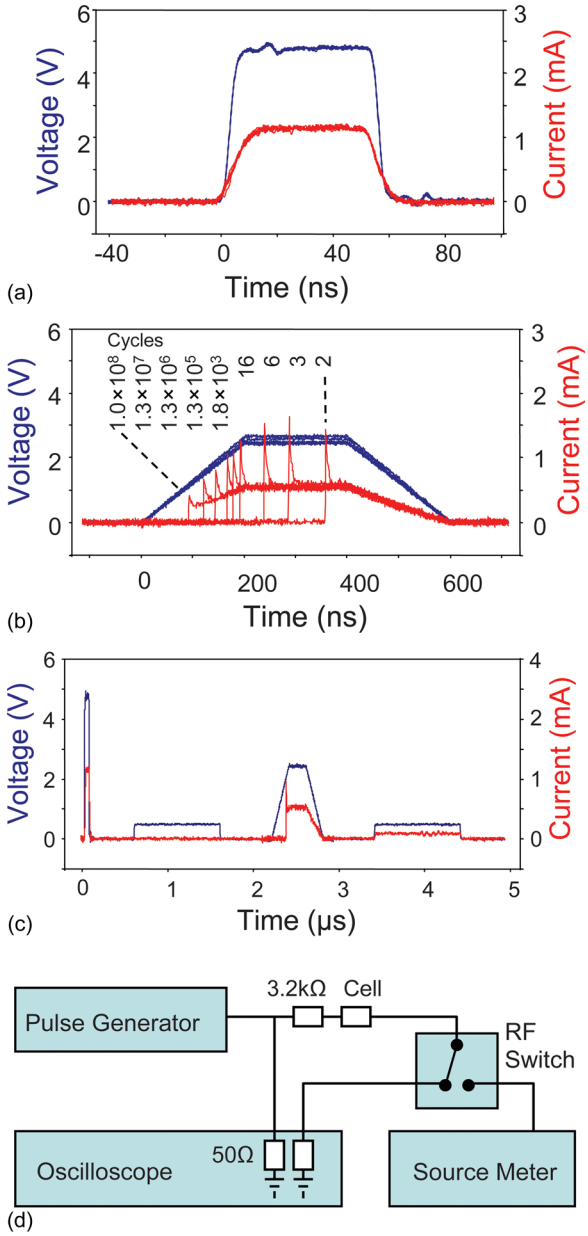

FIG. 2. (Color online) (a) Oscilloscope traces of nine single RESET pulses taken every decade of cycling showing no evolution in the programming current, (b) nine single SET pulses taken throughout cycling, and (c) a fast cycle. The latter consists of four separate oscilloscope traces (one for each pulse) from the same measurement. The apparent lower noise of the read pulses arises from averaging performed internally by the oscilloscope when acquiring traces longer than 250 ns. (d) Setup used for the electrical characterization.

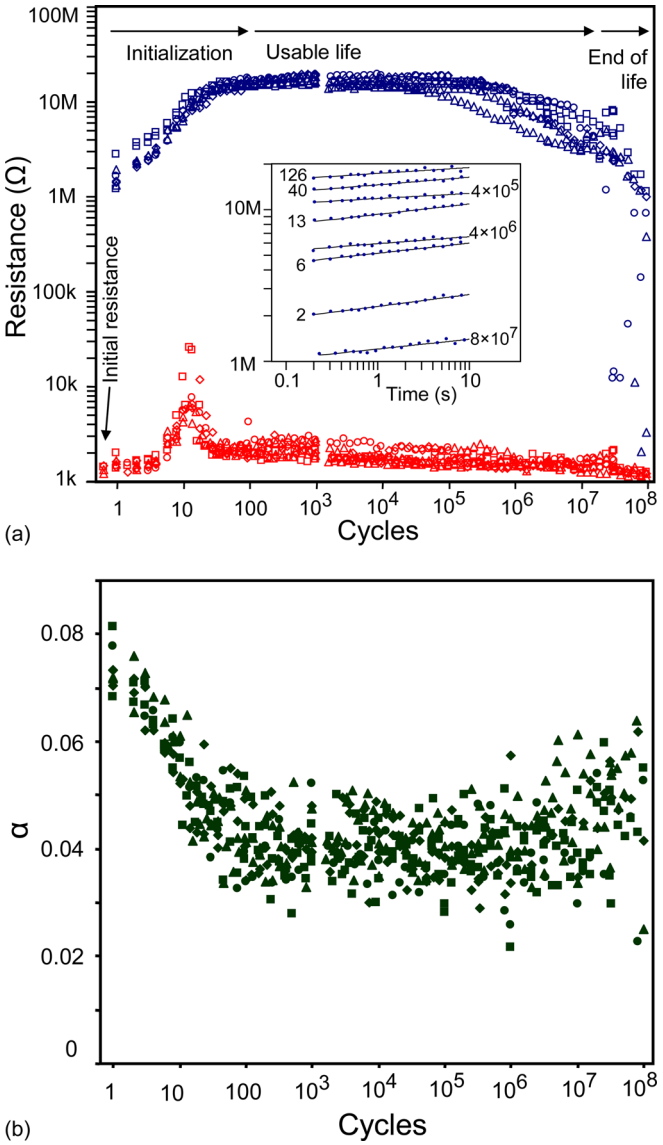

FIG. 3. (Color online) (a) A set of complete switching cycles of seven $15 \times 75 \times 225$ nm^3 line cells. The resistances shown are measured with the source meter after either a single RESET or SET pulse. The amorphous resistance R_1 is always obtained from the time dependent measurement. Inset: A selection of resistance measurements as a function of time (and power law fit) performed at various cycle numbers from which the amorphous resistance R_1 and α were calculated. (b) Drift exponent α measured for the amorphous resistance as a function of the number of switching cycles for the seven cells.

probe system. As the temperature of the cell during the SET pulse is close to (but below) the melting temperature, a capacitive current from a sharp edge (in the mA range) can lead to parasitic RESET.[16] In a real memory application these leading and trailing edges are not necessary because capacitive currents of the selection transistor are orders of magnitude smaller.[16]

B. Fast RESET/SET cycle

The previous accurate single cycle is only practical for tens or maybe hundreds of cycles as the resistance measurement with the source meter and the switching of the RF relay take considerable time. To cycle the cell millions of times a pulse pattern was programmed into the arbitrary function generator consisting of a RESET – read – SET – read pattern [shown in Fig. 2(c)]. The (1 μs) read pulses validated that the cells were *actually* switched. Ten data points were collected for each decade of cycling. (See Fig. 3 in Sec. III.) For each of the data points up to 10 fast cycles were recorded for validation of switching. The read pulses allowed for a resistance (V/I) measurement directly after the RESET and SET pulse. The upper measurement limit of the resistance obtained with the 0.5 V read pulses was ~50 kΩ which is sufficient to distinguish between the amorphous and crystalline state.

C. Isochronal crystallization

The cycle experiment was periodically interrupted to perform one or more isochronal crystallization measurements. The cell is made amorphous with a single RESET pulse. The resistance is measured for 1000 s to allow the cell to drift. The temperature is then increased with a constant ramp rate and the resistance is measured at constant temperature intervals until the cell is crystallized (i.e., when the resistance drops below 10 kΩ). The temperature is returned to 25.0 °C by passive cooling.

The activation energy for crystal growth was obtained from isochronal crystallization measurements with varying ramp rates (ranging from 1 to 60 K/min) employing the so-called Kissinger analysis.[17] Between each thermal measurement 10 *fast cycles*, with identical pulse settings as the general cycling experiment, were performed to bring the cell back to the same state as after cycling (named hereafter by *imprint removal cycle*). The imprint removal cycle between the temperature ramps are applied to ensure that the cell had the same value of R_1 and α for each temperature measurement, i.e., to avoid variations in the retention parameters due to partial crystallization after the isochronal measurement.

D. Threshold voltage measurement

Apart from the threshold voltage measurement performed automatically during the general cycle experiment a separate more elaborate measurement of the threshold voltage was performed at various cycle numbers.

The threshold voltage was measured as a function of delay time: Short delay times ranging between 2.3 and 43 μs were obtained by programming a RESET – read – SET – read pattern into the arbitrary function generator. Longer delay times were obtained from a single RESET and SET pulse from ~5 to 1000 s after the RESET pulse.

Also, the threshold voltage as a function of the RESET pulse height was measured: After a RESET pulse, varying in pulse height, the resistance is measured for 100 s. The cell is then switched back to the crystalline state with a SET pulse from which the threshold voltage is obtained. Between each single threshold voltage measurement an imprint removal cycle was applied.

III. RESULTS

A. RESET/SET resistance

The life cycle of the line cells analyzed for the used program settings are shown in Fig. 3(a), demonstrating that the cells can be switched 10 to 100 million times. The life cycle consists of an initialization phase and a usable life phase until the cell becomes stuck in the SET state [see Fig. 3(a)].[14]

During the initialization phase the amorphous resistance R_1 increases about an order of magnitude from the first to about one hundred cycles. This is accompanied by a measured drop of the drift coefficient α from 0.075 ± 0.007 to 0.04 ± 0.01 during the first 100 cycles [see Fig. 3(b)].

A strong increase of the SET resistance from about 1.3 to 10 kΩ followed by a decrease to ~2 kΩ was observed during the initialization phase [Fig. 3(a)].

The usable life phase is characterized by quite stable cell parameters up to about 3.3×10^5 followed by a strong drop in amorphous resistance on a log scale of cycling. Although the amorphous resistance drops significantly the cell can still be switched. Finally the cell can only be brought to the amorphous state by applying a larger magnitude RESET pulse which is recognized here as the end of life phase.

An important observation is that the current during the RESET pulse was not related to the crystalline resistance prior to the pulse. Figure 2(a) shows that the oscilloscope traces from the nine RESET pulses taken at fixed intervals during cycling overlap considerably. The fact that the pulse voltage traces overlap is trivial but this is not the case for the pulse current traces. Although the crystalline resistance continuously decreases from about 2 to 1 kΩ during the lifetime, the RESET current was 1.1 mA throughout. This translates to an invariable cell resistance of 1.2 kΩ during melting which was the same for each cell presented in Fig. 3.

B. Threshold voltage

The measured threshold voltage as a function of the number of switching cycles is shown in Fig. 4(a). After about 100 cycles the threshold voltage dropped considerably. Figure 2(a) shows that during the initialization phase the threshold event occurred during the flat part of the SET pulse shortening the crystallization time. This shorter crystallization time could in fact simply explain the higher SET resistances during this phase as partial crystallization. But successive SET pulses were applied after the threshold event when the SET resistance exceeded 10 kΩ to fully crystallize the cell. However these pulses did not lead to a lower resistance, i.e., did not fully crystallize the amorphous mark.

During the usable life phase the threshold voltage is nearly constant up to around 10^5 cycles and then starts to decrease significantly. Figure 4(a) also nicely demonstrates that the threshold voltage observed during the SET pulse is dependent on how much time passed after the RESET pulse. The longer the time after the RESET pulse the higher the threshold voltage. This holds for each individual line cell, but does not hold beyond 10^5 cycles when comparing the different cells. This gives Fig. 4(a) a somewhat chaotic appearance beyond 10^5 cycles. However, also in Fig. 3(a) it is observed that some cells show a more rapid decrease in amorphous resistance with cycling than others. Therefore it is interesting to correlate the threshold voltage with the amorphous resistance for the (seven) line cells during their life. The result is shown in Fig. 4(b). The various phases during the life of the line cells can be readily discerned. In the initialization phase the amorphous resistance clearly increases and the threshold voltage slightly decreases. During the usable life phase, the threshold voltage and amorphous resistance drop until finally the cell is stuck in the SET state. An interesting observation is that the data are not chaotic anymore beyond 10^5 cycles. For all cells the threshold voltage 2.3 μs and 11 s after the RESET pulse are now well separated. The threshold voltage and amorphous resistance show a dependence that appears to consist of two linear regimes [Fig. 4(b)]. This observation can be explained

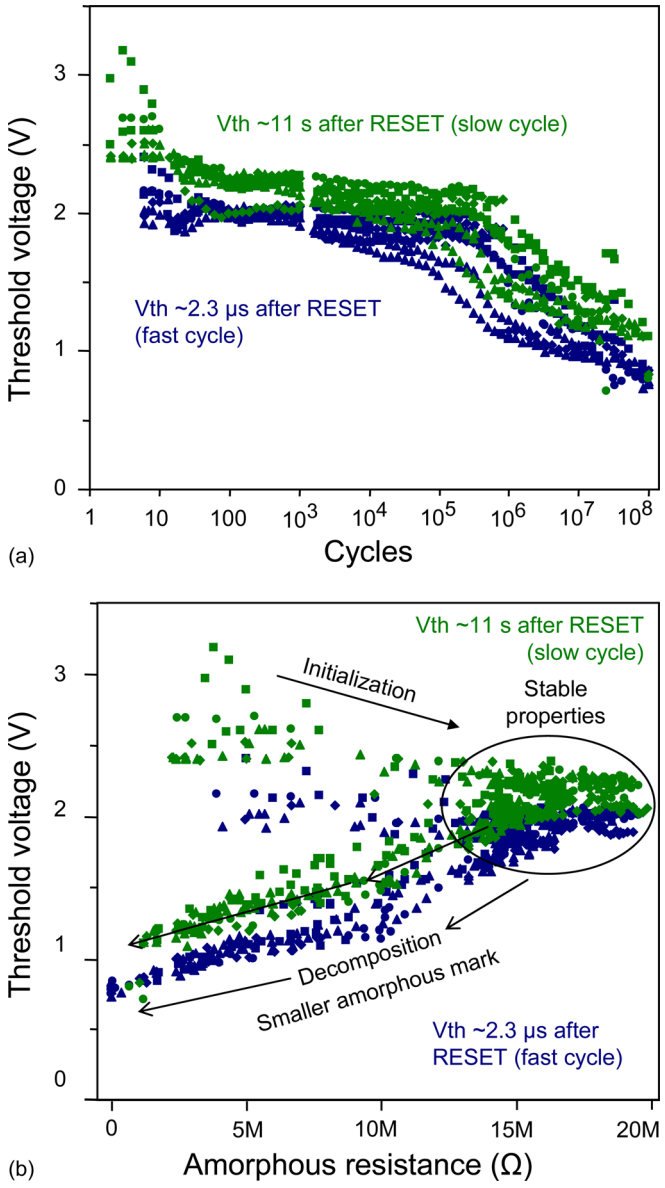

FIG. 4. (Color online) (a) Threshold voltage as a function of cell cycling measured at 2.3 ± 0.1 μs and ~11 s. The uncertainty of the 2.3 μs measurements arises from the fact that the threshold voltage is measured with a 200 ns leading edge: Higher threshold voltages therefore will always have a slightly longer delay time and vice versa. The uncertainty of the measurement at 11 s arises mainly from the reprogramming time of the arbitrary function generator which takes ~1 s (which is added to the 10-s resistance drift time). (b) The threshold voltage from the data of (a) is plotted vs the amorphous-phase resistance from the data of Fig. 3(a). For consistency the amorphous resistance at 1.0 s is plotted. However for the slow cycles, the actual resistance during the SET pulse at which the threshold event takes place (~11 s after RESET) will be 5% to 22% higher depending on the value of α. This difference is very small compared to the evolution the actual resistance values and does not change the observations. Furthermore, during the fast cycles the resistance cannot be measured this accurately and the amorphous resistance of the slow cycle following that particular fast cycle was used.

by two separate processes taking place during the evolution (degradation) of properties induced by cycling.

To gain more understanding on the evolution and behavior of the threshold voltage a more elaborate measurement was performed twice per decade of cycling from 10^3 cycles on. This measurement could not be performed earlier during cycling due to the amount of cycles required for the measurement. Also, as the material properties change quite significantly during the initial 100 cycles such a measurement would generate artifacts caused by the change of properties during the measurement.

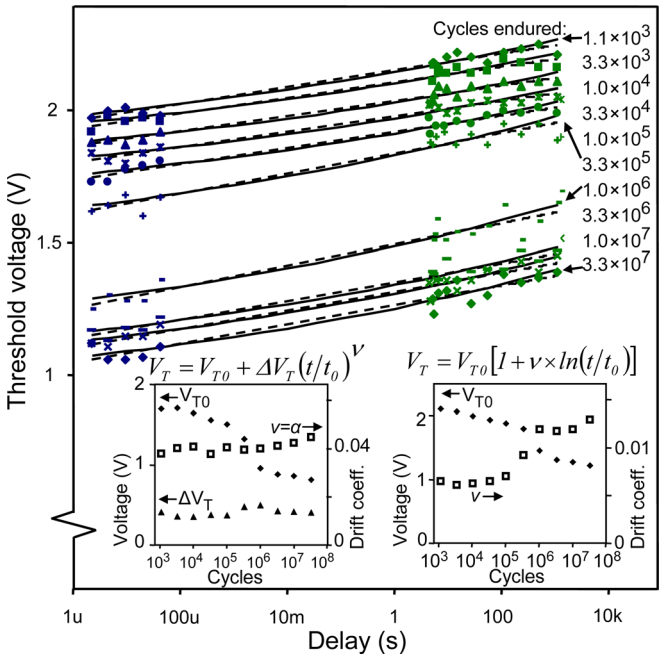

FIG. 5. (Color online) The threshold voltage was measured as a function of time after RESET. The measurement was performed twice every decade of cycling from 1.1×10^3 to 3.3×10^7 cycles. The dotted lines are a fit based on a linear increase in log time (Ref. 10), the solid line is a fit based on a power law (Ref. 9).

Figure 5 shows the time dependence of the threshold voltage after the RESET pulse. The threshold voltage was either measured with a single RESET−read−SET−read pulse or by a single RESET and SET pulse with altered delay time. The total time scale spans nine orders of magnitude. Figure 5 shows that the threshold voltage as a function of time after RESET can be properly fitted with a power law (solid lines) similar to the resistance drift:[8]

$$V_T = V_{T0} + \Delta V_T \left(\frac{t}{t_0}\right)^{\nu}. \tag{1a}$$

This power law was proposed by Ielmini *et al.*[9] and is based on a linear dependence between the threshold voltage and amorphous resistance:[8,9]

$$V_T = V_{T0} + \gamma \times R, \tag{1b}$$

where γ is a fitting parameter. A natural consequence of Eq. 1(b) is that the coefficient of resistance drift and threshold drift necessarily must have the same value. Therefore the threshold drift coefficient ν was set equal to the resistance drift coefficient α, obtained from the resistance drift measurements prior to the threshold event, and the parameters V_{T0} and ΔV_T were fitted to the data (also $t_0 = 1$ s was used). The (left) inset of Fig. 5 shows that both ν and ΔV_T remained fairly constant during cycling: (0.041 ± 0.002) and 0.40 ± 0.05 V, respectively. However, V_{T0} dropped from 1.7 to 0.8 V and follows the general evolution of the threshold voltage of Fig. 4(a). The biggest drop in ΔV_T occurred between 3.3×10^5 and 3.3×10^6

cycles. As the cell continued to be cycled to 3.3×10^7 the value of ΔV_T continued to decrease until finally at 1.0×10^8 cycles the cell was stuck in the SET state.

Our data can also be fitted with the same degree of accuracy to a linear increase of the threshold voltage on a logarithmic time scale (dashed lines) explained by a theoretical model proposed by Karpov *et al.*:[10]

$$V_T = V_{T0}\left[1 + v \times \ln\left(\frac{t}{t_0}\right)\right]. \quad (2)$$

This model explains the increase of threshold voltage by a random double well potential of a metastable disordered atomic structure of a glass. Here the values of V_{T0} and the threshold drift coefficient v are fitted to the data. The (right) inset in Fig. 5 clearly shows that both V_{T0} and v evolve during cycling. V_{T0} which is the threshold voltage at $t_0 = 1$ s, clearly drops significantly which can be expected. However, to keep the slope of the linear fit on log time (fairly) constant v has to increase by an equal amount. A direct consequence is that according to this model the resistance drift, which remains very constant during cycling, does not follow the evolution of the threshold drift coefficient which doubles.

Furthermore, unlike the amorphous resistance that depends directly on a power law, the threshold voltage dependence in both models has the additive constant V_{T0}. Due to this constant both the models of Ielmini and Karpov produce very similar results. We expect that a threshold voltage measurement as a function of delay time of *at least* eleven decades of time are required on cells with high values of α (> 0.07) before the validity of either model can be proven on the basis of such a direct measurement. The fit based on the power law (solid line in Fig. 5) is surprisingly similar to the fit based on a linear increase with log time. Therefore no preference between the models can be made on the basis of the accuracy of our data. However, the model of Ielmini [Eq. (1a)] predicts the evolution of only V_{T0} while the other fit parameter ΔV_T remains fairly constant. The model of Karpov [Eq. (2)] on the other hand implies an evolution of two parameters namely V_{T0} and the threshold drift coefficient v which we consider to be contradictory to the evolution of the resistance drift.

C. Threshold voltage and resistance as a function of pulse height

The threshold voltage and amorphous resistance were measured as a function of RESET pulse height ranging between 3.6 and 6 V (see Fig. 6). RESET pulses with pulse heights lower than 3.6 V were applied, but were unable to bring the cell to the RESET state. This is interesting as it shows that these cells are immediately programmed to a state $> 10^6$ Ω without going into unstable lower resistance intermediate states. The limiting value of 6 V was chosen to avoid damage to the cell. After each individual SET pulse an imprint removal cycle was applied to avoid influencing the next measurement.

During the first 3.3×10^5 cycles the cell behavior was very consistent [Fig. 6(a)]. For pulse heights up to 4.5 V the amorphous resistance increases slightly with pulse height and a decrease in amorphous resistance is observed for pulses larger than 4.5 V. However, the threshold voltage continuously increases with the RESET pulse height leading to the slight, but significant and not yet reported, inverse relation between threshold voltage and amorphous resistance beyond 4.5 V. This inverse relation between the amorphous resistance and threshold voltage can be considered to be an overprogramming artifact related to these cells.

Lacaita *et al.*[18] have observed a linear relation between the amorphous resistance and threshold voltage across a large range (more than an order of magnitude difference) in

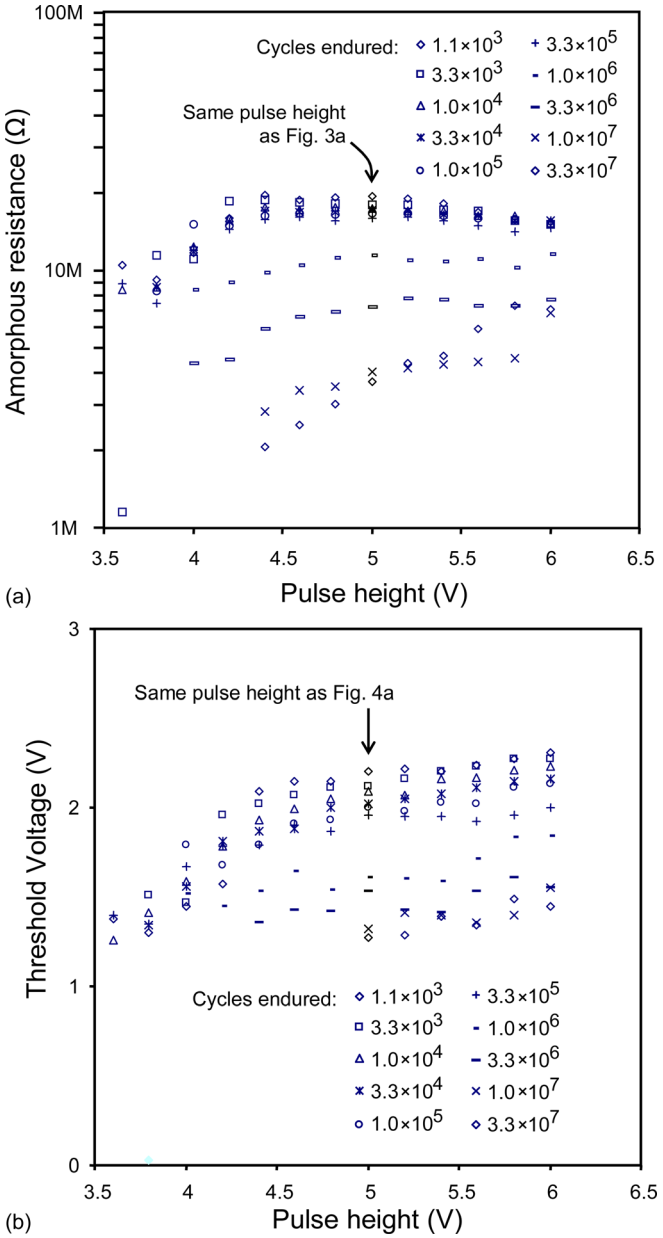

FIG. 6. (Color online) (a) The amorphous resistance was measured for different pulse heights at different cycle numbers. (b) The threshold voltage was measured by applying a SET pulse after the amorphous resistance was monitored for 100 s [see (a)]. Some (low resistance) data points from (a) did not result in a threshold voltage measurement as the cell switched back while latching the RF relay or reprogramming the arbitrary function generator. This shows that the lower resistance states are inherently unstable and can be affected by very small spurious transients.

resistance values. The extrapolation of the threshold voltage to zero amorphous resistance gives the value of V_{T0} on which the model of Ielmini *et al.*[9] is based [Eq. (1a) and (1b)]. Therefore it would be interesting to correlate the evolution of V_{T0} obtained from the threshold voltage drift (Fig. 5 left inset) with values obtained from the threshold voltage [Fig. 6(b)] and amorphous resistance [Fig. 6(a)]. The relation between the amorphous resistance and threshold voltage when varying the pulse height is not a simple linear dependence on these cells. Therefore it is impossible to obtain accurate values of V_{T0} from the data presented in Fig. 6. Moreover, taking into account the varying material properties (within a single fit) it is fundamentally not meaningful to derive V_{T0} from the data in Fig. 6. However, the data of Fig. 5 show that when keeping the programming parameters *constant* it is possible to obtain very reproducible results. The reason is that now the changes in material properties occur between the different fits in Fig. 5 and these changes are reflected in the varying V_{T0} values (Fig. 5 left inset).

As the cell is cycled beyond 3.3×10^5 cycles, the threshold voltage and amorphous resistance both drop significantly and the peak in the amorphous resistance occurs at higher pulse heights. The resistance of the molten region [Fig. 2(a)] and thus the program energy does not change during cycling. Therefore the observations cannot be explained by assuming that a significantly smaller area is molten. The most viable explanation is partial regrowth of the molten region during quenching that leads to a lower resistance and threshold voltage which has also been observed in TEM. This explanation is further supported by the following. Some of the data points in Fig. 6(b) (after 3.3×10^5 cycles), corresponding to lowest resistance values in Fig. 6(a), are missing as the cell crystallized "spontaneously" between the end of the resistance measurement and the application of the SET pulse. Switching the RF-relay and reprogramming (through the GPIB port) of the arbitrary function generator leads to ubiquitous spurious pulses that can crystallize only the most sensitive states i.e. states with a very small amorphous mark.

D. Isochronal crystallization

The crystallization temperature was measured at regular intervals during cycling (see Fig. 7). It was found to continuously decrease during cycling from about 125 °C to 90 °C. This continuous decrease is quite unexpected as the amorphous resistance shows stable values at least in the range from 10^2 to 10^5 cycles [Fig. 3(a)]. In this range the crystallization temperature decreases at least 15 °C. Interestingly, the continuous decrease in crystallization temperature is correlated with a continuous decrease in the threshold voltage (Fig. 7).

The crystallization temperature was also measured with ramp rates (φ) of 1, 2, 4, 8, 15, 30, and 60 K/min [Fig. 8(a)]. The upper inset of Fig. 8(a) shows the resistance-drift curves prior to the temperature ramp, which overlap for a time interval of more than three orders of magnitude. This proves that the cell could be returned to an identical state prior to each temperature measurement.

The activation energy of growth was obtained after the various numbers of cycles from Kissinger plots (figures not shown): The slope of $\ln(\varphi/T^2)$ vs T^{-1} gives the activation energy, which was proven for these cells to be the same as the activation energy obtained from isothermal measurements.[14]

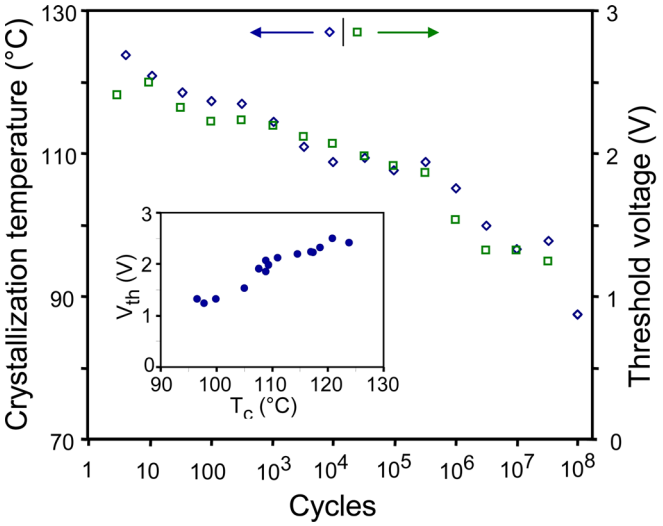

FIG. 7. (Color online) The threshold voltage and the crystallization temperature at a fixed ramp rate (of 30 K/min) vs the number of switching cycles. The crystallization temperature was measured the cycle directly following the threshold voltage and therefore represents a different cycle number. Both the threshold voltage and the crystallization temperature show a strong correlation during cycling (see inset).

The activation energy of growth was found to remain within 2.2 ± 0.2 eV during cycling [see Fig. 8(b)], i.e., no significant evolution with cycling was observed. This is in contrast with the crystallization temperature that shows a relatively dramatic evolution, i.e., decrease with cycling.

IV. DISCUSSION

A. Initialization phase

It was shown in Fig. 3 that the amorphous cell resistance increases sharply during the first one hundred cycles. This increase is accompanied by a decrease of the resistance drift exponent α from 0.075 ± 0.007 to 0.04 ± 0.01. Generally, drift has been attributed to either the dynamics of intrinsic traps[8] or to stress release[19] of the programmed amorphous region of the phase-change material. With each RESET pulse the crystalline to amorphous phase change causes a volumetric expansion of the order of 6%.[20,21] However, also the material surrounding the active phase-change material can respond to and accommodate the volumetric expansion. This accommodation will definitely also occur during the initialization phase and then will not be an effect that is reactivated (RESET) by each RESET pulse, but will be a continuous process like we observed during the first ~100 cycles (see Fig. 3). The fact that we observed such strong initialization effects can be explained by a settle-in/compression of the surrounding (relatively) soft inorganic resist (HSQ) still present on top of these cells. TEM images have confirmed that after the initialization the line narrows at the location of the amorphous mark. As the relatively soft resist is compressed the molten region (with 15×75 nm^2 cross section perpendicular to the current direction) takes a more circular shape due to

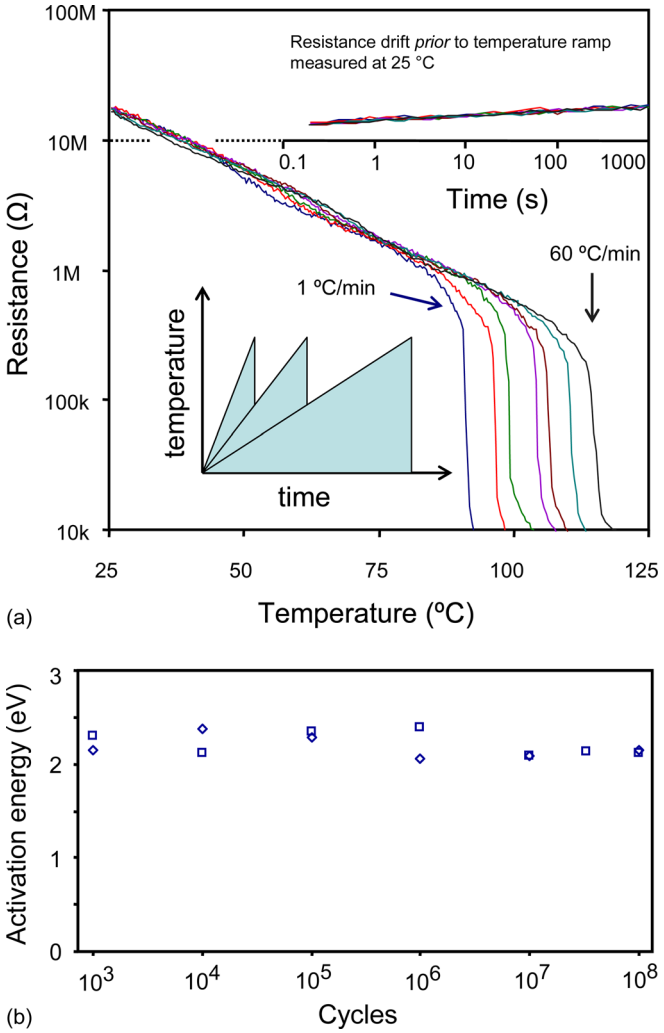

FIG. 8. (Color online) (a) A cell was switched to the RESET state and drifted for 1000 s while the resistance was measured (upper inset). Immediately after the drift period the temperature was raised with a constant ramp rate until the cell crystallized. This was repeated for various ramp rates as schematically depicted in the lower inset (see article text for more details). (b) The activation energy for crystallization (E_C) vs the number of switching cycles. E_C was obtained from the crystallization temperature measured at different ramp rates using the Kissinger analysis. Unlike the crystallization temperature at a fixed ramp rate the activation energy did show a significant evolution during cycling.

surface tension of the molten material. The total surface area of the cross section stays (roughly) the same as the current during melting does not change significantly.

Therefore after each RESET pulse stresses are generated that can subsequently relax in time and can thus be associated with the observed drift. This explanation is consistent with reported drift coefficients of capped and uncapped nanowires that show more drift and much higher values of α when the programmed region is more rigidly constrained.[19] It also explains why in the initialization phase the drift exponent decreases, because the programmed region becomes less constrained. It is important to note that also the increase in amorphous resistance during the first one hundred cycles is consistent with the larger volumetric freedom the active phase change region gets with accommodation of the soft resist. However this view contradicts the experimental evidence of Ref. 8 where resistance drift could be repeated with pulses of insufficient energy to either crystallize or melt the cell.

Therefore, a second explanation is provided that correlates with the experimental evidence presented in this study and of both Refs. 8 and 19: The *actual* increase of the amorphous resistance as a function of time is predominantly related to annihilation of traps, in line with Ref. 8 (although stress release during drift is in principle possible). Stress release or accommodation occurs in the material surrounding the active region during the RESET pulse. The increased stress present at the initial cycles is stable after cooling and during drift. Compressive stress narrows the bandgap of the amorphous state[8] that could lead to a stronger relation between the amorphous resistance and the number of traps, i.e., changing the *value* of the drift coefficient. It is important to note that in both explanations the material surrounding the active region becomes compressed during the first 100 cycles leading to lower compressive stress within the phase-change material. The only difference is whether the drift of the amorphous resistance is directly related to stress release[19] or that the amorphous resistance is a function of the number of traps[8] which is modified by stress.

Within the initialization phase the threshold voltage continuously decreases during cycling. This implies that an inverse relation holds between the threshold voltage and amorphous resistance in the initialization phase. This clearly implies that the increase in amorphous resistance cannot be attributed to merely an increase of the length of the amorphous region in the line cell, but must be related to the increased freedom to expand.

The crystalline resistance shows a large increase followed by a decrease to a value still higher than the initial resistance. However, the resistance during melting (during the RESET pulse) and crystallization (during the SET pulse) do not evolve significantly. Various factors can play a role in this peculiar behavior of the crystalline resistance, but the following explanation appears most consistent.

The initial increase in crystalline resistance is caused by increasing tension in the line as it crystallizes and shrinks, because the PC material in the line remains bonded to the surrounding material that expands (in response to the expansion of the amorphous phase). This is in agreement with the previous explanation for the increasing amorphous resistance and decreasing drift exponent. After a certain number of cycles, corresponding to the maximum in the crystalline resistance, the PC material in the line physically becomes separated from the surrounding material and the crystalline phase is able to relax and can adopt a lower resistance. This separation can be directly observed using TEM[22] as a narrowing (and most likely a thickening) of the line at the location of the amorphous mark.

B. Usable life phase

The cell behavior during the first 3.3×10^5 cycles showed a very consistent behavior [Fig. 6(a)]. For pulse heights up to 4.5 V the amorphous resistance increases slightly with pulse height and a decrease in amorphous resistance is observed for pulses larger than 4.5 V. This anomalous behavior is an

overprogramming artifact: The thermoelectric Thomson effect[23] that was observed on line cells of identical composition (but different processing conditions)[23] causes an asymmetrical thermal distribution in the line during programming. When applying more current than necessary and desirable for switching (overprogramming), part of the amorphous mark will appear partly outside the line and into one flap of the dog bone shaped phase change material. TEM images have confirmed that this is indeed the case.[22] The amorphous region present outside the line that was not programmed before can display initialization effect complicating the analysis.

It is important to note that the conduction mechanism at low carrier concentrations (ohmic region at low read voltages) is fundamentally different from the conduction mechanism at high carrier concentrations. The RESET (and also SET) pulse always leads to a large current density (typically 7×10^{11} A/m^2 during the RESET pulse) and large electric fields ($\sim 10^7$ V/m) within the line cell. During the RESET pulse (and SET pulse), the atoms in the programmed region become mobile.[24–28] Atoms can be ionized and Sb^{3+} and Te^{2-} will move in opposite directions to the electric field. This movement particularly occurs in the molten region during the RESET pulse.[28,29]

A natural consequence of this ionization of mobile atoms is that electromigration will take place during cycling and that the phase-change material will experience decomposition. Our observations show that the usable life phase of the line cell is characterized by a decrease of (i) the amorphous resistance [see Fig. 3(a)], (ii) crystalline resistance [see Fig. 3(a)], (iii) threshold voltage (see Fig. 4), and (iv) crystallization temperature [see Fig. 8(b)]. These observations are indeed consistently explained by decomposition of the programmed region caused by electromigration. During the RESET pulses the ionized atoms move in different directions with respect to the electric field. This will lead to regions enriched in either Sb or Te. Starting from the homogeneous phase-change alloy the decomposed alloy will always lead to a lowering of the crystallization temperature. It will be more difficult to produce amorphous regions in the decomposed material since a part of the melt-quenched region is able to recrystallize. Therefore, with smaller amorphous marks the amorphous resistance and threshold voltage will decrease.[30]

Our measurements clearly indicate that the molten region during the RESET pulse is not affected by cycling; only quenching of this molten state into the amorphous state becomes increasingly difficult beyond $\sim 3.3 \times 10^5$ cycles. Finally amorphous marks cannot be produced (with the standard pulse settings) anymore beyond 10^7 or 10^8 cycles and the cell becomes stuck in the SET state (end of life). This is exactly what we observe and is thus consistently explained by electromigration induced decomposition of the phase-change material. Only with increasing the magnitude of the RESET pulse an amorphous region can be created. The region that melts during the pulse needs to be much larger to accommodate recrystallization. However, then also decomposition is accelerated by the higher programming current.

Figure 6 shows that the RESET pulse height chosen for the majority of the cycles [Fig. 3(a) to 4(a)] was at the maximum amorphous resistance up to 3.3×10^5 cycles where the line is fully amorphous. Afterwards, the decomposition started to become dominant and the shape of the amorphous resistance versus pulse height changed significantly [Fig. 6(a)]. Instead of having a maximum, the amorphous resistance developed a long slope that is explained by partial recrystallization after the RESET pulse. Decomposition fundamentally changes the amorphous structure and crystallization temperature. As the crystallization temperature decreases the cell will naturally spend more time above the crystallization temperature as it melt-quenches. Recrystallization will lead to a smaller amorphous mark that will be more sensitive to ubiquitous spurious pulses ("spontaneous" SET, see Sec. III C and Fig. 6). This is exactly what we observe.

C. Temperature and activation energy of crystallization

The activation energy of crystallization [Fig. 8(b)] did not evolve significantly during cycling, because it is quantified as 2.2 ± 0.2 eV independent of cycling. A strong relation between activation energy and the dielectric material surrounding the phase change material was reported recently.[31] Different activation energies where reported for identical phase change material when either SiO_2 or $ZnS:SiO_2$ where applied as a top layer. Furthermore, line cells with identical composition as reported here but instead capped with a SiO_2 passivation layer yielded an activation energy of 3.3 eV.[32] Therefore the lack of evolution, within the error margin, of the activation energy measured here is an indication that the HSQ capping layer largely determines the activation energy. Phase change line cells of identical composition as presented in this study but capped with SiO_2 had been found to have a higher activation energy of 2.7 eV[33] and 3.0 eV.[32] A decrease in activation energy from 2.4 to 1.75 eV was reported in literature for an increase in Sb content.[30] Although our measurement data were obtained for a much broader ramp-rate range than those of Ref. 30 we believe that isochronal measurement data are needed with a larger range before such a statement can actually be proven. Moreover, we measure in the line cells the combined effect of separate regions becoming enriched in either Te or Sb and therefore the measured activation energy is not directly related to a material with only an increased Sb content.

Figure 7 shows that during cycling the crystallization temperature (measured at a ramp rate of 30 K/min) decreased continuously from 125 °C to 90 °C. This decrease in crystallization temperature is accompanied by a decrease in threshold voltage. Although a reduction in programmed volume (length of the amorphous mark) will lead to a lower crystallization temperature and threshold voltage, it cannot, on its own, explain the drop in both quantities over the complete life of the cells. A reduction of the amorphous mark length of three orders of magnitude would be required to explain the observed change in crystallization temperature which is not in accordance with the observed limited change in threshold voltage and amorphous resistance. However, it can be associated with part of the life cycle, in particular after 3.3×10^5 where recrystallization of the amorphous region is believed to

become apparent (Sec. IV B). Our conclusion is that the threshold voltage and crystallization temperature are both closely related to the decomposition of the amorphous volume (see inset of Fig. 7). The decomposed material, with separate regions enriched in either Sb or Te, exhibits an overall lower crystallization temperature. As a consequence the amorphous-phase resistance and the threshold voltage also decrease. The threshold field, at which electrical breakdown occurs, is known to vary greatly among materials.[2,34] Furthermore, the extrapolated threshold voltage at zero amorphous mark size is finite and also material dependent.[9,11,18,34] The phenomenological threshold voltage is therefore related to both quantities and the length of the amorphous mark. A decrease of both the crystallization temperature and threshold voltage accompanied by a decrease of the amorphous resistivity of almost an order of magnitude was observed for increasing the Sb content in $Sb_xTe_{(1-x)}$ alloys ($x \geq 0.64$)[30] which is consistent without data.

The general view today is that the electrical breakdown during the threshold event is a purely electrical phenomenon.[8,34,35] However, Karpov *et al.*[11] have provided an alternative explanation that relates threshold switching to nucleation of conductive (cylindrical) crystalline filaments induced and stabilized by the electric field. Although the doped SbTe alloy used here[36] is a fast growth material, with little chance of nucleation, the crystallization kinetics at sub-threshold field strength could be fundamentally different. For completeness, we put forward this alternative explanation for threshold switching, because it naturally explains our observation that the threshold voltage is directly related to the crystallization temperature.

V. CONCLUSIONS

This work presents an extensive study on phase change random access memory, and in particular the horizontal line cell geometry.[2] Many cell properties (i.e., the amorphous and crystalline resistances, amorphous resistance drift, threshold voltage, threshold-voltage drift, crystallization temperature, and activation energy for crystallization) were measured during cell cycling on the same cells and can therefore be directly related. Cells can be cycled typically 100 million times and show stable properties after an initialization phase of about 100 cycles up to about 5×10^5 cycles. Beyond this number of cycles the amorphous resistance, the threshold voltage and the crystallization temperature decrease significantly. This behavior is attributed to electromigration induced decomposition of the active phase-change material in the line cell.

Generally, it is assumed and also demonstrated that the threshold voltage (V_T) and the amorphous phase resistance (R_a) are linked in a rigid way. We show that in our measurements the R_a is not the dominating factor for predicting the threshold voltage V_T. By varying the magnitude of the RESET pulse the R_a shows a peak value while the threshold voltage V_T continuously increases leading to both a positive and negative dependence between R_a and V_T. Furthermore, the evolution of the threshold voltage can be linked to the evolution of the crystallization temperature. The crystallization temperature and threshold voltage appear to continuously decrease during cycling due to electromigration induced decomposition and follow a remarkably similar trend.

As the crystallization temperature drops, the molten region can partly recrystallize as it is melt-quenched, i.e., more time is spent above the crystallization temperature leading to smaller amorphous mark, which starts to become apparent after $\sim 3.3 \times 10^5$ cycles. Finally the cell becomes stuck in the SET state after typically 10 to 100 million cycles. Although the material is still molten during the application of a RESET pulse this does not load to an amorphous melt-quenched state as the cell fully crystallizes directly after the pulse.

ACKNOWLEDGMENTS

The research was carried out under project number MC3.05241 in the framework of the Strategic Research program of the Materials innovation institute M2i. Financial support from the M2i is gratefully acknowledged.

We would like to thank Johan Holstein and Siemon Bakker for the use of a probe station that has helped starting up these measurements.

[1] S. Raoux, Annu. Rev. Mater. Res. **39**, 25 (2009).
[2] M. H. R. Lankhorst, B. Ketelaars, and R. A. M. Wolters, Nature Mater. **4**, 347 (2005).
[3] M. Gill, T. Lowrey, and J. Park, Digest of Technical Papers of International Solid-State Circuits Conference, San Francisco, CA (2002), p. 202.
[4] D. H. Im, J. I. Lee, S. L. Cho, H. G. An, D. H. Kim, I. S. Kim, H. Park, D. H. Ahn, H. Horii, S. O. Park, U. I. Chung, and J. T. Moon, in IEEE International Electron Devices Meeting 2008, Technical Digest, New York, (2008), p. 211.
[5] T. Ohta, N. Yamada, H. Yamamoto, T. Mitsuyu, T. Kozaki, J. Qiu, and K. Hirao, Mater. Res. Soc. Symp. Proc. **674**, V1.1.1 (2001)
[6] J. Siegel, A. Schropp, J. Solis, C. N. Afonso, and M. Wuttig, Appl. Phys. Lett. **84**, 2250 (2004).
[7] S. R. Ovshinsky, Phys. Rev. Lett. **21**, 1450 (1968).
[8] A. Pirovano, A. L. Lacaita, F. Pellizzer, S. A. Kostylev, A. Benvenuti, and R. Bez, IEEE Trans. Electron Devices **51**, 714 (2004).
[9] D. Ielmini, A. L. Lacaita, and D. Mantegazza, IEEE Trans. Electron Devices **54**, 308 (2007).
[10] I. V. Karpov, M. Mitra, D. Kau, G. Spadini, Y. A. Kryukov, and V. G. Karpov, J. Appl. Phys. **102**, 124503 (2007).
[11] V. G. Karpov, Y. A. Kryukov, S. D. Savransky, and I. V. Karpov, Appl. Phys. Lett. **90**, 123504 (2007).
[12] Y. Yin, T. Noguchi, H. Ohno, and S. Hosaka, Appl. Phys. Lett. **95**, 133503 (2009).
[13] T. Nirschl, J. B. Phipp, T. D. Happ, G. W. Burr, B. Rajendran, M. H. Lee, A. Schrott, M. Yang, M. Breitwisch, C. F. Chen, E. Joseph, M. Lamorey, R. Cheek, S. H. Chen, S. Zaidi, S. Raoux, Y. C. Chen, Y. Zhu, R. Bergmann, H. L. Lung, and C. Lam, in *Write Strategies for 2 and 4-bit Multi-Level Phase-Change Memory*, (IEEE, Washington, DC, 2007), p. 461.
[14] J. L. M. Oosthoek, B. J. Kooi, K. Attenborough, F. A. M. Hurkx, and D. J. Gravesteijn, Mater. Res. Soc. Symp. Proc., San Francisco, CA, (2010), G14-04-H07-04.
[15] F. J. Jedema, M. A. A. in't Zandt, and W. S. M. M. Ketelaars, Appl. Phys. Lett. **91**, 203509 (2007).
[16] D. Ielmini, D. Mantegazza, A. L. Lacaita, A. Pirovano, and F. Pellizzer, Solid-State Electron. **49**, 1826 (2005).
[17] H. E. Kissinger, Anal. Chem. **29**, 1702 (1957).
[18] A. L. Lacaita, A. Redaelli, D. Ielmini, F. Pellizzer, A. Pirovano, A. Benvenuti, and R. Bez, "Electrothermal And Phase-Change Dynamics In Chalcogenide-Based Memories," in IEDM Tech. Dig. (2004), p. 911.
[19] M. Mitra, Y. Jung, D. S. Gianola, and R. Agarwal, Appl. Phys. Lett. **96**, 222111 (2010).
[20] R. Pandian, B. J. Kooi, G. Palasantzas, J. T. M. De Hosson, and A. Pauza, Adv. Mater. **19**, 4431 (2007).
[21] V. Weidenhof, I. Friedrich, S. Ziegler, and M. Wuttig, J. Appl. Phys. **86**, 5879 (1999).

[22]J. L. M. Oosthoek, B. J. Kooi, F. J. Jedema, K. Attenborough, and D. J. Gravesteijn (in preparation).
[23]D. T. Castro, L. Goux, G. A. M. Hurkx, K. Attenborough, R. Delhougne, J. Lisoni, F. J. Jedema, M. Zandt, R. A. M. Wolters, D. J. Gravesteijn, M. A. Verheijen, M. Kaiser, R. G. R. Weemaes, and D. J. Wouters, "Evidence of the Thermo-Electric Thomson Effect and Influence on the Program Conditions and Cell Optimization in Phase-Change Memory Cells," in IEDM Tech. Dig. (2007), p. 315.
[24]B. Rajendran, M. H. Lee, M. Breitwisch, G. W. Burr, Y. H. Shih, R. Cheek, A. Schrott, C. F. Chen, M. Lamorey, E. Joseph, Y. Zhu, R. Dasaka, P. L. Flaitz, F. H. Baumann, H. L. Lung, and C. Lam, in IEEE Symposium on VLSI Technology, New York, (2008), p. 96.
[25]D. M. Kang, D. Lee, H. M. Kim, S. W. Nam, M. H. Kwon, and K. B. Kim, Appl. Phys. Lett. **95**, 011904 (2009).
[26]C. Kim, D. M. Kang, T. Y. Lee, K. H. P. Kim, Y. S. Kang, J. Lee, S. W. Nam, K. B. Kim, and Y. Khang, Appl. Phys. Lett. **94**, 193504 (2009).
[27]S. W. Nam, D. Lee, M. H. Kwon, D. M. Kang, C. Kim, T. Y. Lee, S. Heo, Y. W. Park, K. Lim, H. S. Lee, J. S. Wi, K. W. Yi, Y. Khang, and K. B. Kim, Electrochem. Solid State Lett. **12**, H155 (2009).
[28]Y. Tae-Youl, P. Il-Mok, K. Byoung-Joon, and J. Young-Chang, Appl. Phys. Lett. **95**, 032104 (2009).
[29]A. Padilla, G. W. Burr, K. Virwani, A. Debunne, C. T. Rettner, T. Topuria, P. M. Rice, B. Jackson, D. Dupouy, A. J. Kellock, R. M. Shelby, K. Gopalakrishnan, R. S. Shenoy, and B. N. Kurdi, IEDM, IEEE International (2010), p. 29.4.1.
[30]M. S. Youm, Y. T. Kim, Y. H. Kim, and M. Y. Sung, Phys. Status Solidi A **205**, 1636 (2008).
[31]F. Jedema, M. in 't Zandt, R. Wolters, and D. Gravesteijn, Jpn. J. Appl. Phys. **50**, 024102 (2011).
[32]J. L. M. Oosthoek, B. J. Kooi, K. Attenborough, F. A. M. Hurkx, and D. J. Gravesteijn, Mater. Res. Soc. Symp. Proc., San Francisco, CA, (2010), G14-04-H07-04.
[33]J. Oosthoek, B. J. Kooi, J. T. M. De Hosson, D. Gravesteijn, K. Attenborough, R. Wolters, and M. Verheijen, Crystallization studies of doped SbTe phase-change thin films and PRAM line cells: Growth rate determination by automated TEM image analysis, Proc. E/PCOS Symp. (2009), p. 140.
[34]D. Krebs, S. Raoux, C. T. Rettner, G. W. Burr, M. Salinga, and M. Wuttig, Appl. Phys. Lett. **95**, 082101 (2009).
[35]A. Redaelli, A. Pirovano, E. Pellizzer, A. L. Lacaita, D. Ielmini, and R. Bez, IEEE Electron Device Lett. **25**, 684 (2004).
[36]J. L. M. Oosthoek, B. J. Kooi, J. T. M. De Hosson, R. A. M. Wolters, D. J. Gravesteijn, and K. Attenborough, Microsc. Microanal. **16**, 291 (2010).